Impact of utility-scale solar photovoltaic array on the aeolian sediment transport in Hobq Desert, China

TANG Guodong, MENG Zhongju, GAO Yong*, DANG Xiaohong

College of Desert Control Science and Engineering, Inner Mongolia Agricultural University, Hohhot 010018, China

Abstract: Deserts are ideal places to develop ground-mounted large-scale solar photovoltaic (PV) power station. Unfortunately, solar energy production, operation, and maintenance are affected by geomorphological changes caused by surface erosion that may occur after the construction of the solar PV power station. In order to avoid damage to a solar PV power station in sandy areas, it is necessary to investigate the characteristics of wind-sand movement under the interference of solar PV array. The study was undertaken by measuring sediment transport of different wind directions above shifting dunes and three observation sites around the PV panels in the Hobq Desert, China. The results showed that the two-parameter exponential function provides better fit for the measured flux density profiles to the near-surface of solar PV array. However, the saltation height of sand particles changes with the intersection angle between the solar PV array and wind direction exceed 45°. The sediment transport rate above shifting dunes was always the greatest, while that around the test PV panels varied accordingly to the wind direction. Moreover, the aeolian sediment transport on the solar PV array was significantly affected by wind direction. The value of sand inhibition rate ranged from 35.46% to 88.51% at different wind directions. When the intersection angle exceeds 45°, the mean value of sediment transport rate above the solar PV array reduces to 82.58% compared with the shifting dunes. The results of our study expand our understanding of the formation and evolution of aeolian geomorphology at the solar PV footprint. This will facilitate the design and control engineering plans for solar PV array in sandy areas that operate according to the wind regime.

Keywords: aeolian sediment transport; mass flux density profiles, sand-fixation; shelter efficacy; solar photovoltaic array

1 Introduction

Solar photovoltaic (PV) technology is one of the most important means used by many countries to wean themselves off the dependence on conventional fossil fuel-based energy sources and reduce greenhouse gas emissions(Garcia et al., 2014). China's desert area is about 7×10^5 km^2, of which sandy land area is about 5×10^5 km^2 and accounts for 13% of the country's total land area (Li et al., 2020). Most of the deserts are distributed in arid and semi-arid areas in Northwest China, which have rich solar and thermal resources (Li et al., 2006; Li and He, 2010; Shen et al., 2013). These desert areas are largely unsuitable for activities such as agriculture (Mani and Pillai, 2010), and

*Corresponding author: GAO Yong (E-mail: 13948815709@163.com)

TANG Guodong and MENG Zhongju contributed equally to this work.

Received 2020-08-17; revised 2020-11-20; accepted 2021-01-13

hence the cost of using the land is very low. Thus, deserts are ideal places to build ground-mounted utility-scale solar PV power stations in China (Huang et al., 2018). This has the potential to improve the land utilization rate and produce economic benefits. In 2018, the world's solar power generation was 2480.4 TWH, with China's contribution being 634.2 TWH. However, deserts are characterized by strong winds, sand activities and surface mobility. Solar energy production, operation and maintenance are affected severely by the geomorphological changes caused by the surface erosion process after the construction of large-scale solar PV power station. Most previous studies have focused on designing efficient structures to withstand aerodynamic forces (Kopp and Surry, 2002; Mani and Pillai, 2010; Kopp et al., 2012; Schellenberg et al., 2013; Warsido et al., 2014; Jubayer and Hangan, 2014, 2016; Shademan et al., 2014) and influence PV power generation efficiency by dust deposition on PV panels (Nahar and Gupta, 1990; Said, 1990; Al-hasan et al., 2005; Elminir et al., 2006; Cabanillas and Munguia, 2011; Adinoyi and Ghoneim, 2013; Appels et al., 2013; Zorrilla-Casanova et al., 2013; Boyle et al., 2015; Etyemezian et al., 2017). Yet, there is limited information about the aeolian sand transport processes and surface erosion of PV facilities in desert areas.

Many desert surfaces, especially those with high silt and clay contents, are much more prone to wind erosion when mechanically disturbed (Houser and Nickling, 2001; Macpherson et al., 2008). Lands are disturbed when utility-scale solar facilities are built. The field surface air flow characteristics can be altered with the installations of PV facilities, resulting in further loss of soil under the surface of PV panels and formation of sand ridge landforms between the panels. The geomorphological changes of PV power stations caused by the surface erosion processes can aggravate the release rate of surface dust and increase the dust deposition on PV panels. In addition, erosion can expose the panel column base and lead to instability of the PV panel infrastructure. Thus, it is necessary to investigate the characteristics of wind-sand movement under the interference of solar PV array to avoid further damage to the solar PV power station and plan how to control sand using engineering means.

Aeolian transport is the basic process that defines the evolution of aeolian geomorphology (Lü et al., 2016). In order to understand the characteristics of sediment transport under the interference of solar PV array, more effective measures should be taken to control and improve the movement of sand flow for the purpose of eliminating harm. Significant efforts have been made in the sediment transport theory, and there are mathematical models for mass-flux-density profiles over different underlying surfaces. Different methods have also been established for wind-tunnel tests and field observations. Although there is no consensus on the best mathematical model for the horizontal sediment flux, it is now widely accepted that the mass-flux-density of suspended sediment decaying with increasing height follows a power function (Zingg, 1953; Ni et al., 2002). and the mass flux density of saltating sediment decaying with increasing height follows an exponential decay function (Namikas, 2003; Ellis et al., 2009; Mertia et al., 2010; Dong et al., 2011; Dong et al., 2012; Zhang and Dong, 2014; Zhang et al., 2017). However, establishing the solar PV array can disrupt this relationship. In most previous research that focused on wind tunnel and numerical simulation tests, the height of the solar panel above the ground and the aspect ratio (width/breadth) did not have a significant effect on the aerodynamic coefficients of the panel. And the row spacing for a ground-mounted solar panel array and wind direction had a significant effect on the wind load and wind flow field characteristics of the panel (Inc, 1980; Kopp et al., 2012; Shademan et al., 2014; Warsido et al., 2014; Jubayer and Hangan, 2016). However, little work has been done to compare sand transport with different wind directions in solar PV power stations in sandy areas. Likewise, field experience has shown that the intensity of erosion and deposition are also different in different parts of the solar PV power station and the windward edge area is stronger than the hinterland area of the solar PV array (Guo et al., 2018). This study systematically analyses the mass-flux-density profile and the aeolian transport rate of sediment transport around the PV panels in the hinterland of solar PV array with different wind directions. Our overall goal was to provide information that could be used to determine the technical scheme of wind-sand hazard prevention and control in solar PV power stations to ensure safe and stable operation of the plant.

2 Methods

2.1 Study area and the test PV power station

The study area was located at the middle part of the Hobq Desert in China (37°20′–39°50′N, 107°10′–111°45′E; Fig. 1). The area has a typical temperate continental climate, with mean annual precipitation of 227 mm and mean annual potential evaporation of 2400 mm. The mean annual solar radiation in the area is 597.9 KJ/cm^2 and the annual mean wind velocity is 3.5 m/s. The wind direction is primarily from the west or northwest, with the strongest winds occurring in March to May. Long-term surface aeolian sand activity processes lead to the formation of aeolian landforms including crescent dune, crescent dune chain and lattice dune chain.

Our test solar PV power station was built at the end of 2018. The relative mechanical leveling work was carried out before the installation of the PV panels. The capacity of the solar PV power station was 200 MW-p and covered an area of 5.9 km^2. The size of a single group of PV panels was 18 m×4 m and consisted of 2 rows and 18 columns of basic panel cell (1 m×2 m). The upper edge of the panel was 2.70 m and the down edge was 0.35 m above the ground. Each panel had a projection width of 3.2 m. The PV panels faced south with an inclination of 36°. The north-south spacing between the panels was 8 m. Our observation field was 300 m from the west edge of the solar PV power station. During the test, the surface of the power station did not have any protective measures such as sand-binding plants or sand-barriers.

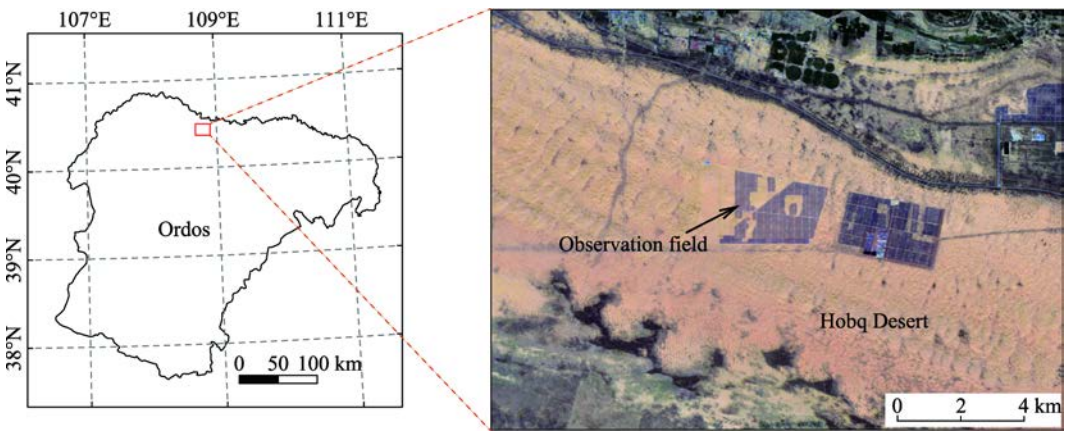

Fig. 1 Location of the study area (a) and its satellite image (b)

2.2 Observation methods

Aeolian sand activity was strongest within the study area during March–May due to the frequent occurrence of strong wind, extended drought and limited rain (Fig. 2). Thus, in this study, field observations were conducted from 20 March to 13 April 2019. To investigate the influence of wind direction on the characteristics of wind-sand movement of solar PV array, we collected the sediment transport data at eight wind directions (Fig. 3; Table 1). After each observation, the change in the shape of the underlying surface was noted. Wind erosion led to the formation of trenches in the immediate vicinity of the downwind of the panels and sand ripples between adjacent north-south panels (Fig. 4a). The changes in the micro-topography likely influenced wind speed characteristics and sand transport. Thus, we smoothened the surface surrounding the test PV panels and flattened the underlying surface before the experimental instruments were arranged (Fig. 4b–c). This was undertaken to allow the comparison of the experimental results.

The configuration of specific measurement instruments is shown in Figure 4d. We established four observation sites. Three observation sites were around the PV panels: one between the panels, one before the panels, and one behind the panels. The fourth observation site was set up on shifting dunes free of the solar PV array in the west, which was 300 m from the solar PV power station. With one sediment sampler at each observation site, the sampler was about 0.3 m tall, and was

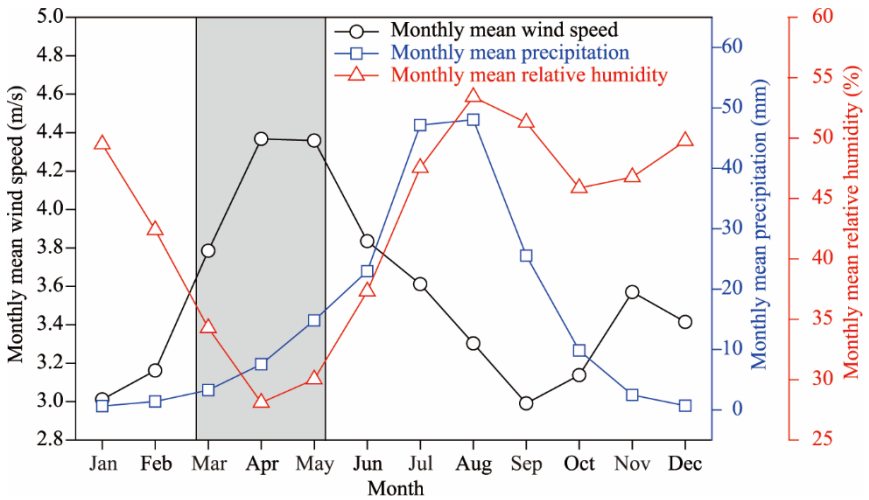

Fig. 2 Meteorological data for period 1980–2018 in Yikewusu Meteorological Station in Hangjin Banner, Ordos City, Inner Mongolia Autonomous Region, China. The grey area in the figure was the best time to investigate the aeolian sand movement in the field due to the frequent occurrence of strong wind, extended drought and limited rain.

Table 1 Field observation data

Prevailing wind direction		Intersection angle (°)	Mean wind speed (m/s)	Observation time		Surface vegetation coverage
				Date	Time (LST)	
A	W, WSW	−12.30	11.57	5 April 2019	10:30–11:20	0
B	W	9.13	11.07	5 April 2019	12:09–12:39	0
C	W, WNW	10.71	10.46	5 April 2019	13:30–14:00	0
D	WNW	18.07	7.73	5 April 2019	17:05–17:35	0
E	WNW, NW	29.67	7.37	5 April 2019	15:55–16:25	0
F	NW, NNW	61.61	7.92	4 April 2019	16:45–17:45	0
G	NNW, N	78.45	9.75	8 April 2019	17:10–17:40	0
H	N	82.19	8.71	13 April 2019	16:30–16:50	0

Note: W, west; WSW, west-southwest; WNW, west-northwest; NW, north-west; NNW, north-northwest, N, north. In this study, we designated W wind direction as parallel solar PV array, that is, the intersection angle between solar PV array and wind direction is 0°. N or S (south) wind direction is vertical to PV array, that is, the intersection angle is ±90°. According to this, we calculated the intersection angle of wind direction and solar PV array.

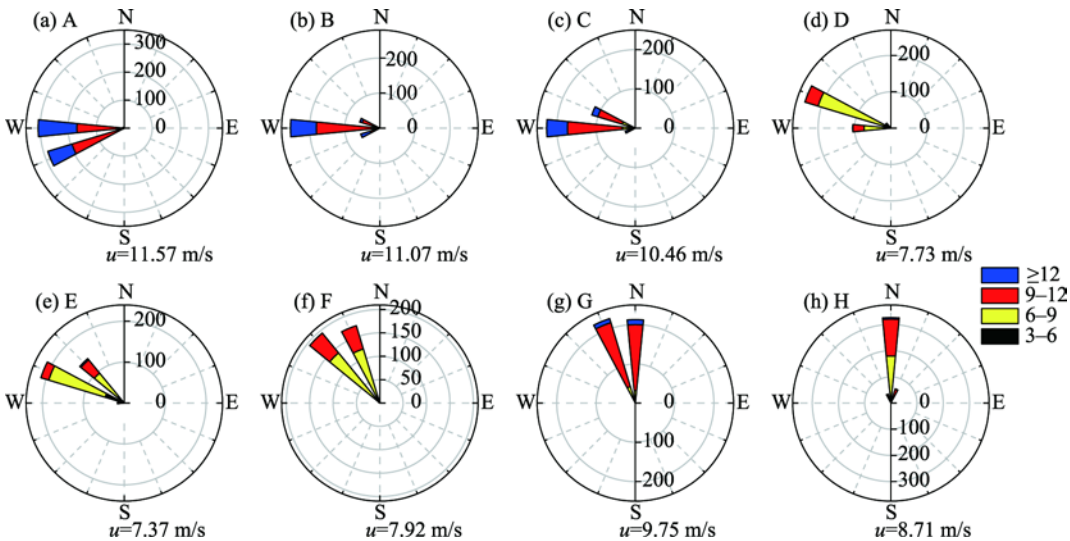

Fig. 3 Wind speed and direction corresponding to sand transport events. *u* represents the free-stream wind velocity at 2 m above the shifting dunes. A–H represent the eight prevailing wind directions in Table 1, respectively.

divided into 15 vertical openings (0.02 m×0.02 m for each) that performed the collection of horizontally transported, wind-eroded sediment above the surface (Fig. 4e). The time duration of the individual observations were 20 to 60 min. These were determined by the magnitude of the sediment transport rate, whereby the greater the transport rate, the shorter the duration of observation. For each measurement period, we measured the sand transport in all four locations at the same time, from the beginning to the end of the sand transport period. We used an electronic balance with 0.01-g precision to weigh the transported sediments collected at each height. Wind speed and wind direction were recorded using a HOBO sensor (Onset Computer Corp., USA) at the observation sites of shifting dunes and between the panels. This was done synchronously with the Aeolian sediment transport observation. Cup anemometers were arranged at heights of 20, 50, 100 and 200 cm. Wind vane was installed at a height of 200 cm. The acquisition interval was 3 s.

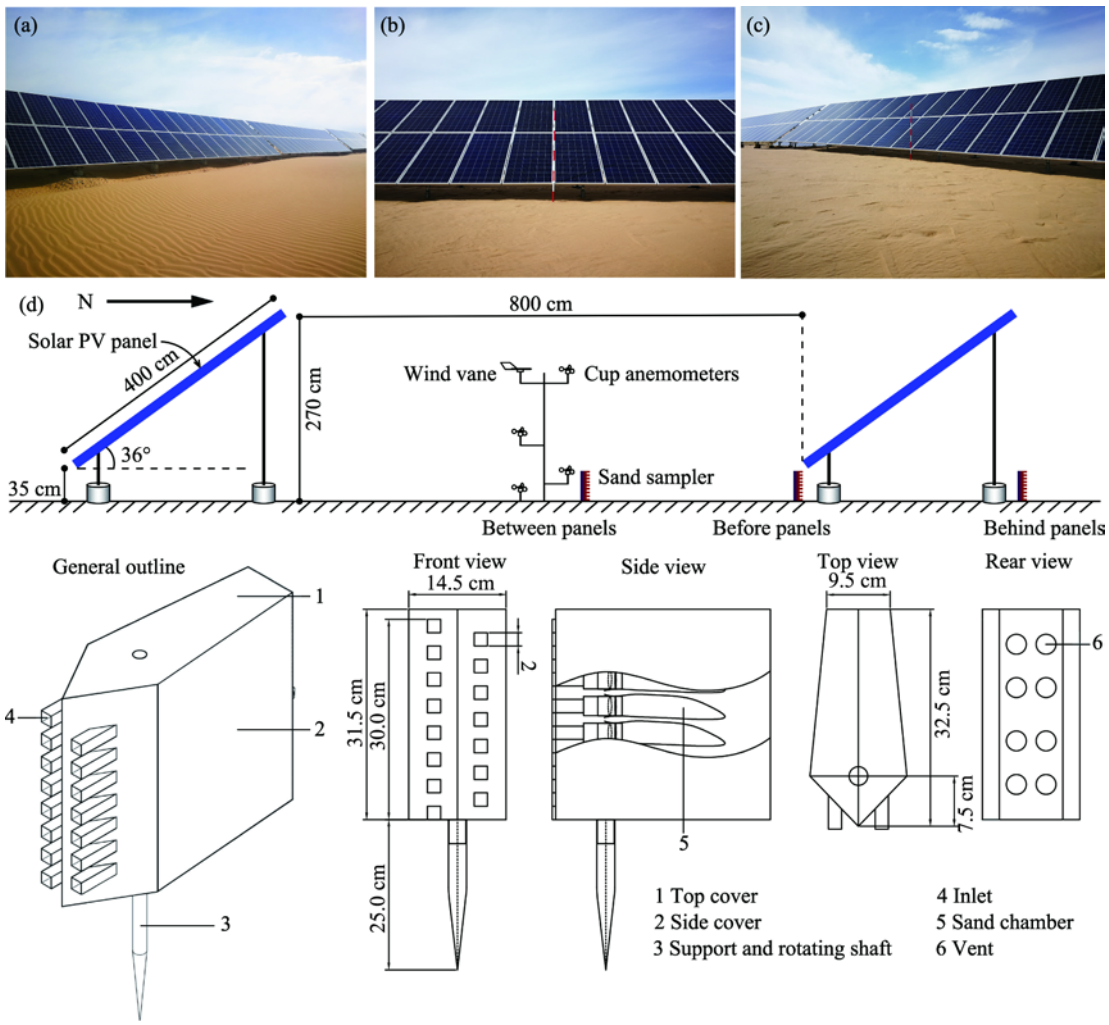

Fig. 4 Surface morphology of the test PV (photovoltaic) panels before the experiment (a), surface morphology after smoothening the surface surrounding the test PV panel (b and c), configuration diagrams of specific measurement instrument (d), and illustration of the test sand sampler (e)

2.3 Data Analysis

2.3.1 Calculation of the mass flux density profiles

The mass-flux-density profile describes how the sand transport rate (mass per unit time and per unit area) changes with the increase in height above the ground. Although there is no consensus on the best mathematical model for the horizontal sediment flux, exponential, power and modified

functions of multi-parameters usually produce better results. Thus, we selected the three commonly used models to investigate the mass flux density profiles above solar PV power station surface.

$$q(z) = a_1 z^{-b_1}, \tag{1}$$

$$q(z) = a_2 e^{-z/b_2}, \tag{2}$$

$$q(z) = c_3 + a_3 e^{-z/b_3}, \tag{3}$$

where the height z represents the arithmetic mean of the top and bottom of each chamber in the sampler (cm); $q(z)$ represents the flux at height z (g/(cm^2·min)); a and b represent regression coefficients.

2.3.2 Calculation of aeolian environment effect

The average wind speeds varied during the observation period of eight wind directions (Fig. 3), and ranged from 7.37 to 11.57 m/s. In order to eliminate the differences in sediment transport caused by different wind speeds during the observation period of eight wind directions, the interception effect solar PV array on sediment transport are expressed by the sand inhibition rate.

$$R_q = \frac{q_{st} - q_{PV}}{q_{st}}, \tag{4}$$

where R_q represents the sand inhibition rate, q_{st} represents the aeolian sediment flux above shifting dunes, and q_{PV} represents the average aeolian sediment flux (g/(cm^2·min)) of three observation sites around the PV panels.

Similarly, we used the relative acceleration rate to show the effect of the solar PV array on the near-surface wind speed (Jackson and Hunt, 1975).

$$R_u = \frac{u_z - u'_z}{u_z}, \tag{5}$$

where R_u represents the relative acceleration rate, u_z represents the measured velocity (m/s) at z height above shifting dunes, u'_z represents the measured velocity (m/s) at z height (cm) of the solar PV array.

3 Results

3.1 Mass-flux-density profiles

The relationship between the sand transport rate and height are shown in Figure 5 under conditions of the eight wind directions. The sand transport rate decay with the height increasing. Table 2 shows the results of the regression analyses for the mass-flux-density profiles above shifting dunes and three observation sites around the PV panels at eight wind directions. We found that the three-parameter modified exponential function in Equation 3 provides the best fit to the observed mass density profiles. However, this improvement of fit was very limited to the observed mass flux density profiles compared with the two-parameter exponential function in Equation 2. The regression goodness of fit (R^2) in Equation 2 was greater than 0.97 in all cases. In more than 84% of the cases, the correlation coefficient (R^2) was greater than 0.99. Therefore, we prefer Equation 2 because it contains fewer coefficients to be defined. That is to say, the existence of solar PV array does not change the sediment transport rate model around the PV panel (between, before and behind the panels). The two-parameter exponential function provides adequate description of the aeolian flux density profiles under the interference of solar PV array in the sandy area investigated.

Most previous studies show that the parameter a in Equation 2 represents the maximum value of the flux density, while other studies suggest that the parameter a represents creeping in the sediment transport (Dong et al., 2002). The relationships between regression coefficient a and wind direction are shown in Figure 6a. The coefficient a decreases as the wind direction changes from W (west) to N (north). The parameter b in Equation 2 represents the decay rate of sediment transport as a function of height (Dong et al., 2002). The greater the value of b, the more slowly the flux density

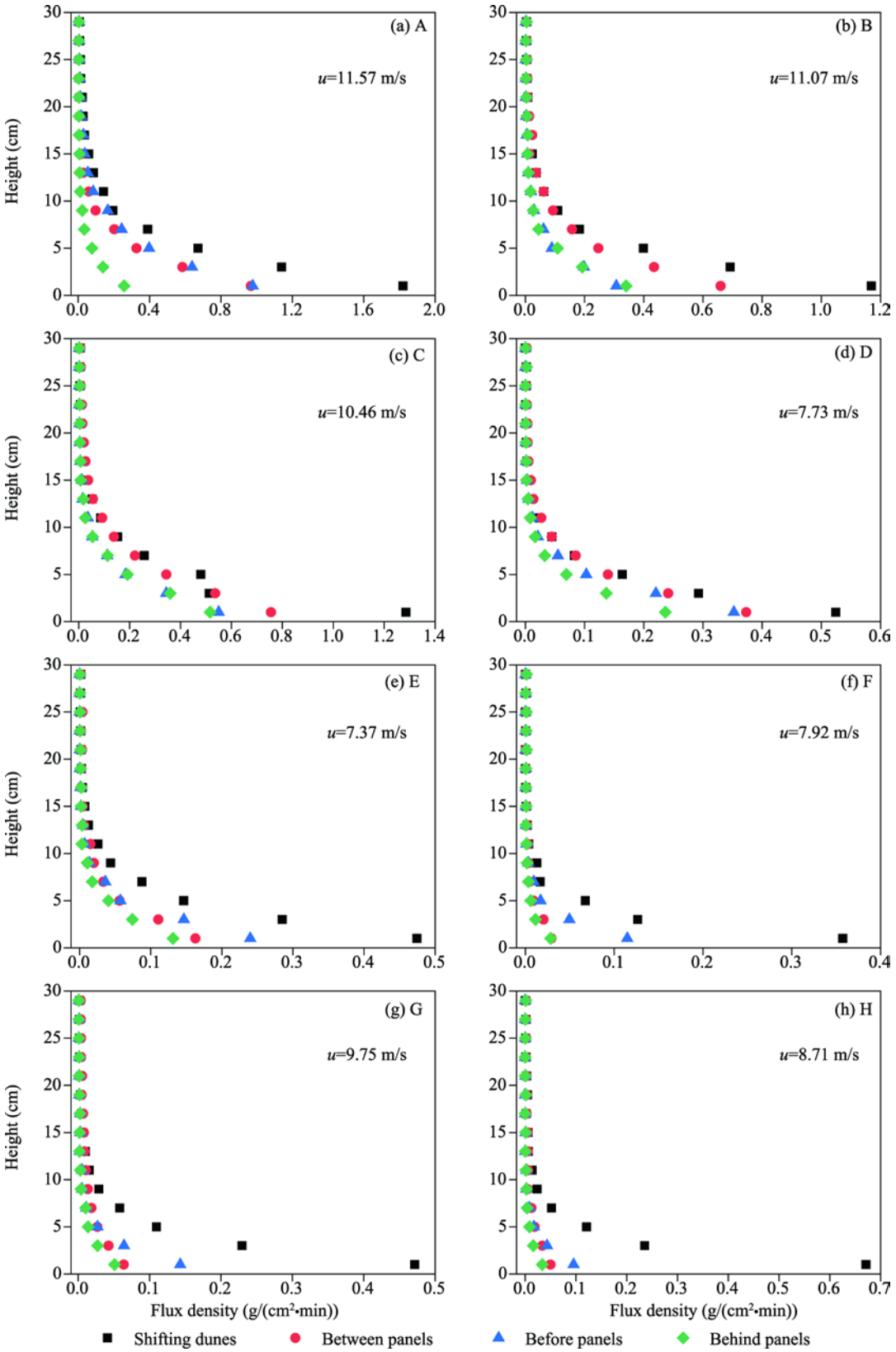

Fig. 5 Variation with height in the observed aeolian sediment flux above the shifting dunes and three observation sites of solar PV array at eight wind directions. Note that the *x*-axis scales differ between observation periods.

decays with height. From Figure 6b, we can see that the value of *b* has a slow decrease trend as the wind direction changes from WSW (west-southwest) to N except for observation site between the panels.

Table 2 Results of the regression analyses for the mass-flux-density profiles above shifting dunes and three observation sites of solar PV array at eight prevailing wind directions calculated using Equations 1–3

WD	OS	Equation 1 ($q(z)=a_1 z^{-b_1}$)			Equation 2 ($q(z)=a_2 e^{-z/b_2}$)			Equation 3 ($q(z)=c_3+a_3 e^{-z/b_3}$)			
		a_1	b_1	R^2	a_2	b_2	R^2	$a_3\times100$	b_3	c_3	R^2
A	CK	1.9360	0.8830	0.9107	2.3689	3.9293	0.9989	0.3580	0.4220	0.7741	0.9989
	TP	1.0245	0.9162	0.9153	1.2771	3.7037	0.9993	–0.2280	0.7833	0.7650	0.9993
	FP	1.0489	0.8385	0.9003	1.2385	4.3745	0.9993	0.0220	0.8074	0.7955	0.9993
	HP	0.2679	0.9632	0.9427	0.3501	3.2383	0.9979	0.3080	2.8458	0.7253	0.9991
B	CK	1.2336	0.9354	0.9185	1.5671	3.5273	0.9985	–0.0578	0.6382	0.7535	0.9985
	TP	0.7061	0.8522	0.9036	0.8462	4.1982	0.9984	0.2040	1.1813	0.7861	0.9984
	FP	0.3265	0.9200	0.9072	0.4131	3.6049	0.9945	–0.0110	2.4207	0.7580	0.9945
	HP	0.3567	0.9568	0.9302	0.4632	3.3179	0.9976	0.2100	2.1556	0.7354	0.9979
C	CK	1.3176	0.9585	0.9524	1.6331	3.4843	0.9723	1.5740	0.6079	0.7397	0.9735
	TP	0.8222	0.7891	0.8799	0.9451	4.8709	0.9982	–0.0484	1.0581	0.8147	0.9982
	FP	0.5839	0.9114	0.9092	0.7291	3.7175	0.9983	–0.1450	1.3721	0.7659	0.9983
	HP	0.5561	0.8788	0.8804	0.6866	3.9526	0.9929	–0.3620	1.4569	0.7805	0.9932
D	CK	0.5498	0.9682	0.9283	0.7105	3.3367	0.9997	–0.1200	1.4083	0.7427	0.9997
	TP	0.3988	0.8776	0.9002	0.4862	4.0000	0.9984	–0.1140	2.0572	0.7807	0.9984
	FP	0.3730	0.9657	0.9036	0.4870	3.3311	0.9943	–0.2820	2.0555	0.7459	0.9948
	HP	0.2483	0.9810	0.9219	0.3265	3.2258	0.9981	–0.0715	3.0647	0.7356	0.9982
E	CK	0.5009	0.9389	0.9183	0.6373	3.5112	0.9988	–0.0851	1.5699	0.7534	0.9988
	TP	0.1745	0.8695	0.8984	0.2141	3.9698	0.9943	–0.0787	4.6685	0.7744	0.9944
	FP	0.2527	0.9921	0.9120	0.3370	3.1437	0.9928	–0.1280	2.9709	0.7312	0.9931
	HP	0.1378	0.9704	0.9276	0.1799	3.2680	0.9983	0.0184	5.5556	0.7354	0.9983
F	CK	0.3628	1.2286	0.9778	0.5717	2.1030	0.9970	0.1020	1.7452	0.6187	0.9971
	TP	0.0314	0.8722	0.9000	0.0391	3.8197	0.9848	0.0449	25.4453	0.7598	0.9863
	FP	0.1174	1.1737	0.9642	0.1785	2.2774	0.9990	0.0150	5.5960	0.6435	0.9991
	HP	0.0289	1.0558	0.9836	0.0417	2.5246	0.9860	0.0913	23.4192	0.6407	0.9968
G	CK	0.4869	1.0464	0.9559	0.6722	2.8058	0.9996	0.2750	1.4839	0.6954	0.9999
	TP	0.0680	0.7121	0.9411	0.0732	5.6786	0.9751	0.4300	13.3333	0.7940	0.9980
	FP	0.1465	1.1075	0.9662	0.2148	2.4582	0.9984	0.1470	4.6318	0.6567	0.9994
	HP	0.0530	0.9343	0.9545	0.0681	3.3580	0.9923	0.1240	14.5349	0.7230	0.9970
H	CK	0.6807	1.2092	0.9831	1.0664	2.1231	0.9969	0.4990	0.9317	0.6166	0.9975
	TP	0.0534	0.7944	0.9171	0.0627	4.4783	0.9796	0.2050	15.7978	0.7727	0.9898
	FP	0.0980	1.1354	0.9597	0.1445	2.4307	0.9994	0.0066	6.9204	0.6621	0.9994
	HP	0.0348	1.0271	0.9586	0.0475	2.8727	0.9968	0.0386	20.9205	0.6964	0.9979

Note: WD, wind direction; OS, observation site; CK, shifting dunes; TP, between panels; FP, before panels; HP, behind panels. *a* and *b* represent regression coefficients.

3.2 Sediment transport rate and thickness of the saltation layer

Figure 7 shows the sediment transport rate above the four observation sites at eight wind directions. The sediment transport rate above shifting dunes is always larger than that in the solar PV array in all cases, and the gap between them was large among the different wind directions. The amount of the shifting dunes was 1.55 times that of the mean value of the solar PV array with the prevailing

wind direction of WNW, while it was 8.70 times with the prevailing wind direction of N. It can be seen that the amount of kinetic energy obtained by the near-surface of solar PV array is strongly related to the wind direction. With the change in wind direction from W to N, less and less kinetic energy was transmitted to the near-surface and the role of solar PV array to intercept wind sand flow became more pronounced.

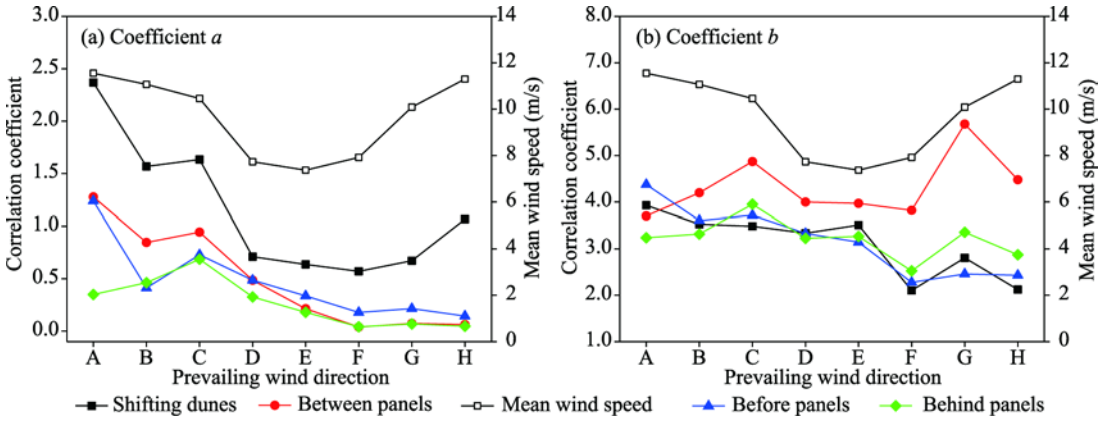

Fig. 6 Relationship between regression coefficient *a* and *b* of the two-parameter exponential function (Equation 2) for the mass-flux-density profiles and the observed wind direction and wind speed

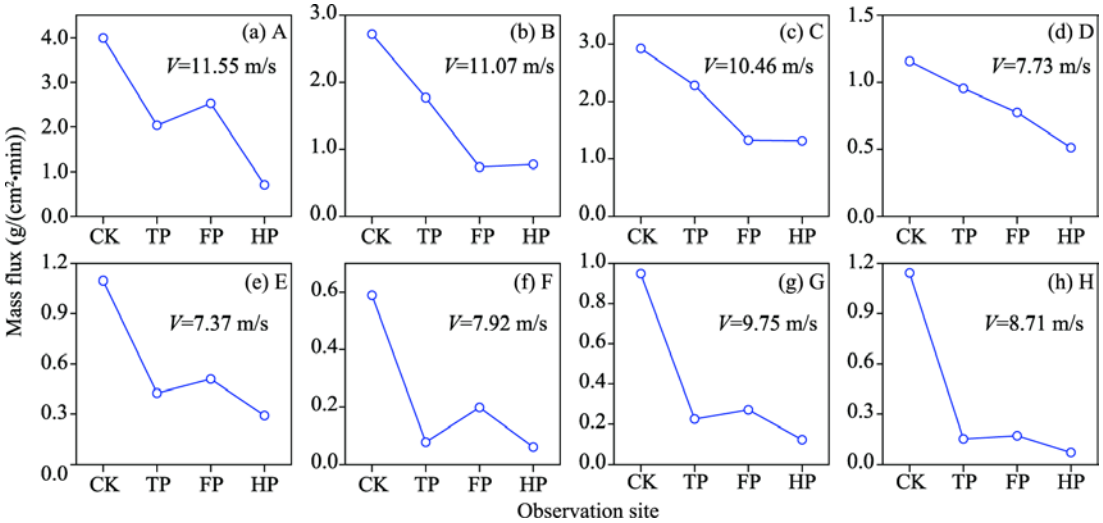

Fig. 7 Sediment transport rate (*V*) at eight prevailing wind directions above the shifting dunes and three observation sites of solar PV array. CK, shifting dunes; TP, between panels; FP, before panels; and HP, behind panels.

In the solar PV array, the amount of sediment transport rate for three observation sites was also related to the wind direction. It was highest in the observation site between the panels and lowest in the case of sites before and behind the panels when the prevailing wind direction was almost parallel to the arrangement direction of the solar PV array (Fig. 7b and c). With the positional relationship between wind direction and solar PV array changing from parallel to vertical, the sediment transport rate increased for the observation site before the panels and decreased for the observation site between the panels. Then, the amount of sediment transport rate increased to the highest point in the observation site before the panels (Fig. 7a, e–h), followed by the sites between and the behind-panels.

To further understand the relationship between the sand transport and height under the interference of solar PV array, we have plotted the cumulative histograms for the four observation sites at eight wind directions (Fig. 8). Most of the sand is transported very close to the ground in all cases with the prevailing wind direction of WSW, W or WNW (Fig. 8a–e). It is also shown that

75 % and 90% of the total transport is concentrated below 0.05m and 0.1m, respectively. It can be seen that vertical distribution of sand transport has not been impacted by the solar PV array under these conditions. Wind sand flow for the sites between and behind the panels tended to move towards a high layer evidently with the prevailing wind direction of NW, NNW or N (Fig. 8f–h), 75% and 90% of the total transported particles was concentrated below 0.10 and 0.20 m, respectively. However, the saltation height in the observation site before the panels tended to move towards a low layer, with 75% and 90% of the total transported particles being concentrated below 0.03 and 0.06 m, respectively.

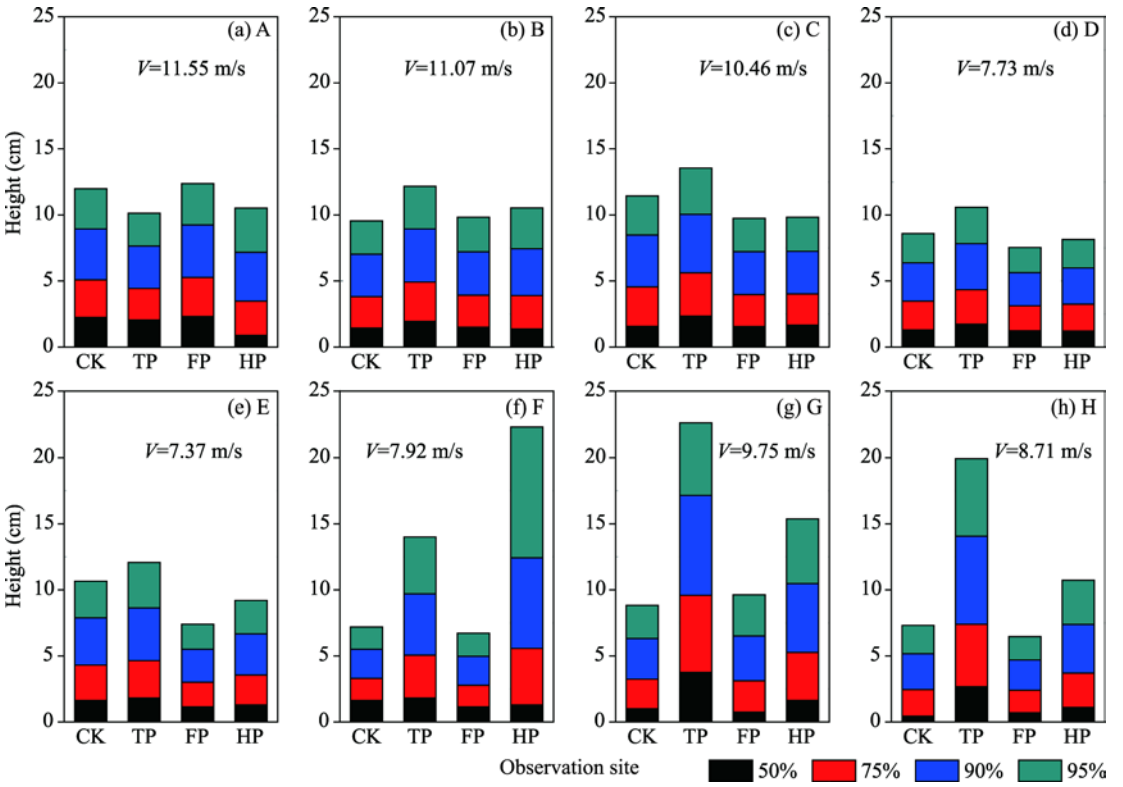

Fig. 8 Cumulative percentage of sand transported above the shifting dunes and three observation sites of solar PV array at eight prevailing wind directions

3.3 Sand inhibition rate of utility-scale solar PV array

The relationship between the sand inhibition rate and wind direction are shown in Figure 9. The sand inhibition rate was significantly affected by the wind direction, with the value ranging from 35.46% to 88.51% at different wind directions. It was the lowest for the prevailing wind direction of WNW and highest for the prevailing wind direction of N. The sand inhibition rate decreased initially before increasing when the prevailing wind direction changed from W to N (Fig. 9b–h), it has a downward trend with the wind direction from W to WNW (Fig. 9b–d) and increases quickly with the addition of NW wind direction. And it goes a step further to increase when the prevailing wind direction was NW (northwest), NNW (north-northwest) or N, with the mean value of up to 82.58%. In contrast, we found that the sand inhibition rate varied when the wind direction changed from W to WSW and WNW. It was 56.01% with prevailing wind direction of WSW and W (Fig. 9a), and only 43.88% and 35.46% with prevailing wind direction of WNW and W, respectively (Fig. 9c and d). These differences are caused by the structural characteristics of PV facilities, the PV panels are face south, hence high in the north and low in the south, and incline at an angle of 36°. The airflow was more directed to the surface after being blocked by the solar PV array when the wind direction was WNW, while it was more directed to the upper atmosphere direction with the wind direction of WSW. It can be seen that the sand inhibition rate for the wind direction of

WSW is better than that for the wind direction of WNW due to the difference in the kinetic energy obtained by the near-surface of the solar PV array.

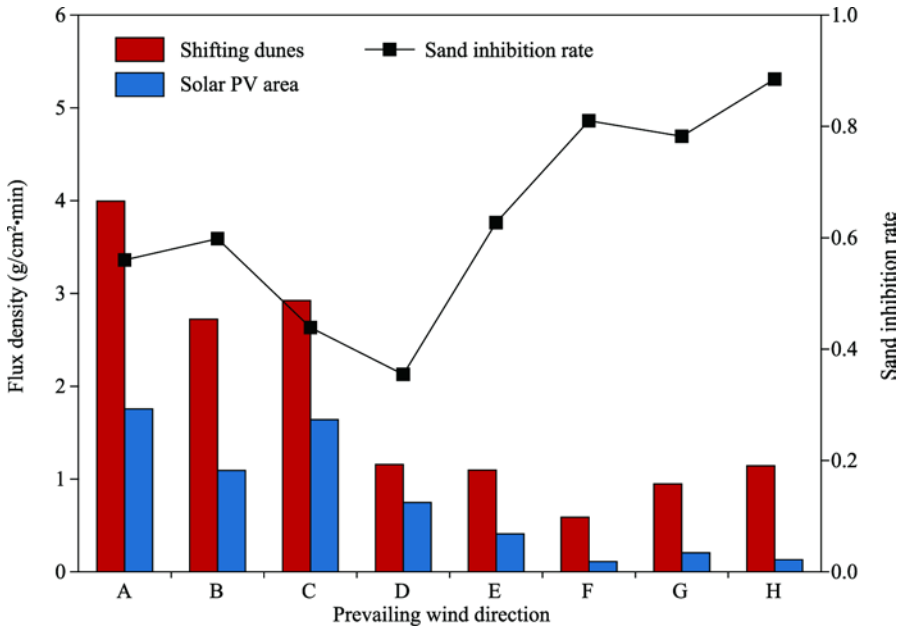

Fig. 9 Sand inhibition rate above the shifting dunes and three observation sites of solar PV array at eight prevailing wind directions

4 Discussion

The field studies are crucial to improve our understanding of sediment transport under the interference of solar PV array. Meanwhile, they can support the theoretical analyses and verify the results from numerical simulations. Previous studies (Zingg, 1953; Ni et al., 2002; Dong et al., 2011; Zhang et al., 2017) have suggested that an exponential function, a power function or their modified function is the most suitable for expressing the horizontal sand flux. In the present study, we found that two-parameter exponential function provides adequate description of the aeolian flux density profiles for the shifting dunes and three observation sites around the PV panels in all case. That is to say, the existence of solar PV array does not change the sediment transport rate model. However, the saltation height of sand particles was affected by solar PV array, and it was related with the intersection angle. The saltation height did not change significantly with the intersection angle less than 45°, but increased significantly for the sites between and behind the panels and decreased in the case of the observation site before the panels with the intersection greater than 45°. These differences may have resulted from differences in characteristics of the wind regime such as turbulence and vortex. The numerical simulation (Jubayer and Hangan, 2016) test shows that there is almost no vortex in the solar PV array when the prevailing wind direction was NW or NS. There was vortex when the prevailing wind direction was N or S (especially N). Meanwhile, the saltation height declined in the sites before the panels (out of the lower edge of PV panels). This was due to the oblique downward flow guide action as the PV panels became stronger with the intersection angle increasing.

Further the mean wind speed of eight prevailing wind direction observation periods ranged from 7.73 to 11.57 m/s due to uncontrollable field conditions. We attempted to investigate the effect of wind speed on the saltation height of the sand particles. When there is an obvious change in the saltation height changes obviously, the corresponding the wind speeds are 7.92, 8.71 and 9.75 m/s for Figure 8f–h, respectively. Conversely, before the saltation height changes, the wind speeds are 7.37, 7.73, 10.46 11.07 and 11.55 m/s for Figure 8e, d, c, b and a, respectively. Consequently, wind speed did not play a decisive role in the saltation height of the sand particles.

The sediment transport rate, the height of the sand transport and the regression coefficient *a* were affected by wind speed (Dong et al., 2012; Lü et al., 2016; Zhang et al., 2016;). It has been established that the value of a increases with the increase in the wind speed, while the value of b has no obvious relationship with wind speed (Zhang and Dong, 2013). The result of our observations above shifting dunes in the present study supports this finding (Fig. 10). In Figure 6a, the wind speed corresponding to the regression coefficient *a* under different wind directions is different. The value of *a* for the wind direction A–C should be lower than the current measured value and that of the wind direction D–E should be higher than the current value in Figure 6a. If we consider the effect of wind speed on the value of *a* and modified it by the relationship between coefficient *a* and the wind speed. Obviously, this does not break the whole tendency of regression coefficient *a* with the wind direction changing. It can be seen that the creeping sediment transport decreases as the intersection angle increases above the surface in the solar PV array.

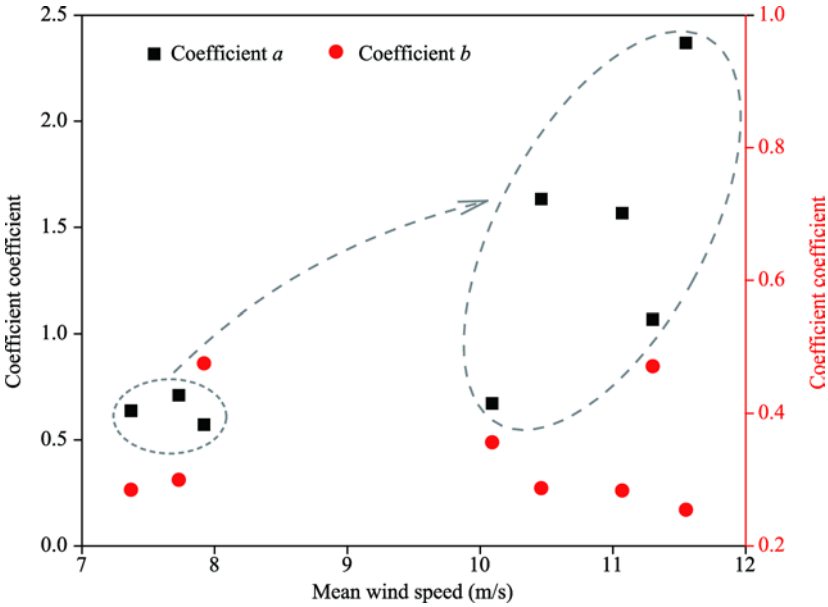

Fig. 10 Relationship above shifting dunes between regression coefficients *a* and *b* in Equation 2 and the wind speed

Table 3 Relative acceleration rate (R_u) of wind speed at different heights above the surface in the solar PV array

Height (cm)	R_u							
	A	B	C	D	E	F	G	H
20	0.21	0.28	0.28	0.11	0.28	0.66	0.67	0.63
50	0.15	0.18	0.14	0.01	0.21	0.63	0.69	0.64
100	0.14	0.14	0.07	–0.04	0.22	0.63	0.66	0.62
200	0.15	0.11	0.10	0.10	0.26	0.59	0.66	0.60

Note: A–H represent the prevailing wind directions.

Our field observations confirmed that the sediment transport rate for solar PV array was influenced by the intersection angle. It was 48.42% of that above the shifting dunes when the intersection angle was less than 45°, and 17.42% when the intersection angle exceeded 45°. Obviously, the intersection angle between the solar PV array and wind direction is a key factor impacting on the sediment transport in the solar PV array.

Wind provides the power that entrains sediments and thereby creates aeolian geomorphology and shapes its subsequent development (Zhang et al., 2015). Recently, numerical simulation (Jubayer and Hangan, 2016) and field observation (Etyemezian et al., 2017) studies have shown that the attenuation of wind is maximal as the intersection angle approaches 90° regardless of the forward or reverse winds. This is consistent with the research results of this paper. We used relative

acceleration rate of wind speed to provide a measure for evaluating the change of air flow at heights of 20, 50, 100 and 200 cm above the surface under solar PV array disturbance. Table 3 shows the relative acceleration rate of wind speed of the solar PV array in the hinterland region at eight wind directions. Clearly, differences in wind directions affect the relative acceleration rate. The rate ranged from 0.11 to 0.23 when the angle between the wind direction and solar PV array was less than 45°, and it ranged from 0.62 to 0.65 when the angle was more than 45°. We used linear regression analysis for the relationship between the sand inhibition rate and the relative acceleration rate at heights of 20, 50, 100 and 200 cm above the surface (Fig. 11). We found that the relationship was strong and significant at each height. The regression goodness of fit (R^2) was greater than 0.82 in all cases. This can better explain the difference of sediment transport under different wind directions.

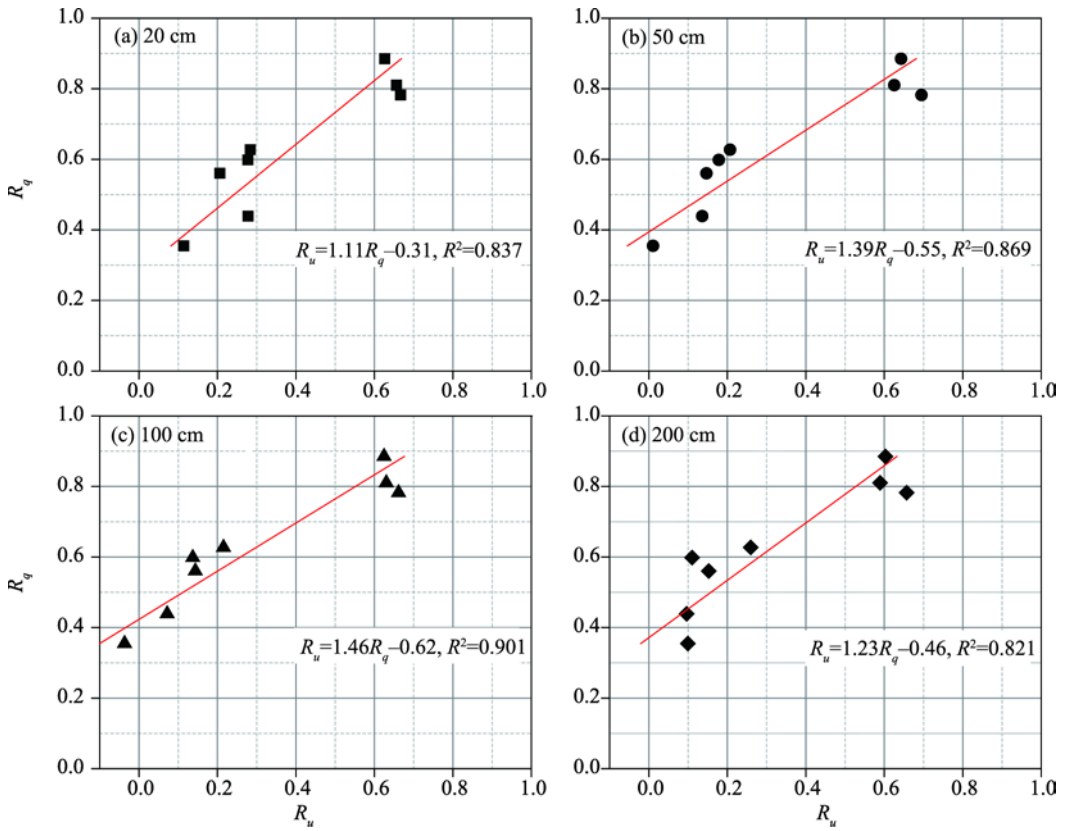

Fig. 11 Relationship between the sand inhibition rate (R_q) and the relative acceleration rate (R_u) at heights of 20, 50, 100 and 200 cm above the surface of solar PV array calculated using Equations 4 and 5, and the result of linear correlation between them.

We conclude that the aeolian sediment transport has a significant correlation with the free-stream wind direction of the environment. When the intersection angle exceeds 45°, the solar PV array itself can effectively play a role in sand-fixation and shelter efficacy. This effect was very limited with the intersection angle of less than 45°, resulting in the loss of soil more easily under the surface of the solar PV array. This information could then be used to determine prevention and control technical schemes for the solar PV footprint. For the solar PV array of panels facing south and east-west arrangement, in response to the wind direction of NNW, N, NNE, SSE, S and SSW, we need to focus on the near-surface sand control engineering measure for the edge zone of north and south. In response to the wind directions of SW, WSW, W, WNW, NW, NE, ENE, E, ESE and SE, we need to set up sand barriers in the solar PV array east and west sides to reduce the wind energy. This is also effective for the protection of the edge zone. It should be noted that the sand barrier needs to play an important role in reducing wind energy entering the solar PV array, not only sand

fixing. Hence, the sand barrier configuration can be an upright sand fence protective belt, or a combination of upright sand fence and checkerboard sand barriers. Certainly, the sand barrier could also be replaced by facilities with similar functions. Meanwhile, we could be also plan protection engineering structures for solar PV array in sandy areas according to the wind regime. For example, our study solar PV array was located in Northwest China, where the primary-harm wind direction is the W or NW. Therefore, the protection engineering structures in west side of the solar PV array should be better than that in east side.

5 Conclusions

Utility-scale solar PV power station in desert areas is one of the most important growth points in the development of clean energy in recent years. Detailed field observations of the flux of wind-blown sediment under the interference of solar PV power station, enable the definition of the near-surface mass flux density profiles, which help us to plan sand control engineering structures for solar PV footprint in sandy areas according to the wind regime.

It was found that the existence of solar PV array does not change the sediment transport rate model. The two-parameter exponential function provides adequate description of the aeolian flux density profiles under the interference of solar PV array. However, with the intersection angle increasing, the saltation height of sand particles for the sites between and behind the panels increased significantly. The saltation height decreased in the case of the observation site before the panels.

The sediment transport rate above shifting dunes was always the greatest. By contrast, it reduced by 51.58% above the solar PV array when the intersection angle was less than 45° and 82.58% when the intersection angle exceeded 45°. This shows that the aeolian sediment transport above the solar PV array was affected significantly by the free-stream wind direction of the environment.

Acknowledgements

This research was supported by the Major Science and Technology Projects of Inner Mongolia Autonomous Region of China (zdzx2018058-3), the National Key Research and Development Project of China (2016YFC0500906-3), the Scientific and Technological Innovation Guiding Fund Project of Inner Mongolia Autonomous Region of China (R&D and Demonstration of Ecological Deserticulture Technology of Solar Photovoltaic Power Station in Sand Area) and the Scientific Research Project of Universities in Inner Mongolia Autonomous Region of China (NJZY19052).

References

Adinoyi M J, Said S A M. 2013. Effect of dust accumulation on the power outputs of solar photovoltaic modules. Renewable Energy, 60: 633–636.

Al-hasan A, Ghoneim A. 2005. A new correlation between photovoltaic panel's efficiency and amount of sand dust accumulated on their surface. International Journal of Sustainable Energy, 24(4): 187–197.

Appels R, Lefevre B, Herteleer B, et al. 2013. Effect of soiling on photovoltaic modules. Solar Energy, 96: 283–291.

Bechtel National, Inc. 1980. Wind design of flat panel photovoltaic array structures. Sand 79–7057. Springfield: National Technical Information Service, U S Department of Commerce.

Boyle L, Flinchpaugh H, Hannigan M P. 2015. Natural soiling of photovoltaic cover plates and the impact on transmission. Renewable Energy, 77: 166–173.

Cabanillas R E, Munguia H. 2011. Dust accumulation effect on efficiency of Si photovoltaic modules. Journal of Renewable and Sustainable Energy, 3(4), doi: 10.1063/1.3622609.

Dong Z, Liu X, Wang H, et al. 2002. The flux profile of a blowing sand cloud: a wind tunnel investigation. Geomorphology, 49(3–4): 219–230.

Dong Z, Lu J, Man D, et al. 2011. Equations for the near-surface mass flux density profile of wind-blown sediments. Earth Surface Processes and Landforms, 36(10): 1292–1299.

Dong Z, Lü P, Zhang Z, et al. 2012. Aeolian transport in the field: A comparison of the effects of different surface treatments. Journal of Geophysical Research: Atmospheres, 117(D9). doi.org/10.1029/2012JD017538.

Ellis J T, Li B, Farrell E J, et al. 2009. Protocols for characterizing aeolian mass-flux profiles. Aeolian Research, 1(1–2): 19–26.

Elminir H K, Ghitas A E, Hamid R H, et al. 2006. Effect of dust on the transparent cover of solar collectors. Energy Conversion and Management, 47(18–19): 3192–3203.

Etyemezian V, Nikolich G, Gillies J A. 2017. Mean flow through utility scale solar facilities and preliminary insights on dust impacts. Journal of Wind Engineering and Industrial Aerodynamics, 162: 45–56.

Garcia E T, Ogueta-Gutierrez M, Avila S, et al. 2014. On the effects of windbreaks on the aerodynamic loads over parabolic solar troughs. Applied Energy, 115: 293–300.

Guo C, Han Z, Li A, et al. 2018. Dynamic mechanism research on the secondary blown sand disaster in the 110-MW photovoltaic arrays of the Hobq Desert. Journal of Desert Research, 38: 225–232.

Houser C A, Nickling W G. 2001. The emission and vertical flux of particulate matter <10 mm from a disturbed clay-crusted surface. Sedimentology, 48(2): 255–267.

Huang B, Li Z, Zhao Z, et al. 2018. Near-ground impurity-free wind and wind-driven sand of photovoltaic power stations in a desert area. Journal of Wind Engineering and Industrial Aerodynamics, 179: 483–502.

Jackson P S, Hunt J C R. 1975. Turbulent wind flow over a low hill. Quarterly Journal of the Royal Meteorological Society, 101(430): 929–955.

Jubayer C M, Hangan H. 2014. Numerical simulation of wind effects on a stand-alone ground mounted photovoltaic (PV) system. Journal of Wind Engineering and Industrial Aerodynamics, 134: 56–64.

Jubayer C M, Hangan H. 2016. A numerical approach to the investigation of wind loading on an array of ground mounted solar photovoltaic (PV) panels. Journal of Wind Engineering and Industrial Aerodynamics, 153: 60–70.

Kopp G A, Farquhar S, Morrison M J. 2012. Aerodynamic mechanisms for wind loads on tilted, roof-mounted, solar arrays. Journal of Wind Engineering and Industrial Aerodynamics, 111, 40–52.

Kopp G A, Surry D. 2002. Wind loads on a solar array. Wind and Structures, 5(5), 393–406.

Li K, He F. 2010. Analysis on mainland China's solar energy distribution and potential to utilize solar energy as an alternative energy source. Progress in Geography, 29: 1049–1054.

Li S, Li C, Yao D, et al. 2020. Feasibility of microbially induced carbonate precipitation and straw checkerboard barriers on desertification control and ecological restoration. Ecological Engineering, 105883, doi: 10.1016/j.ecoleng.2020.105883.

Li X R, Xiao H L, He M Z, et al. 2006. Sand barriers of straw checkerboards for habitat restoration in extremely arid desert regions. Ecological Engineering, 28(2): 149–157.

Lü P, Dong Z, Ma X. 2016. Aeolian sand transport above three desert surfaces in northern China with different characteristics (shifting sand, straw checkerboard, and gravel): field observations. Environmental Earth Sciences, 577, doi: 10.1007/s12665-016-5361-7.

Macpherson T, Nickling W G, Gillies J A, et al. 2008. Dust emissions from undisturbed and disturbed supply-limited desert surfaces. Journal of Geophysical Research, 113(F2), doi: 10.1029/2007JF000800.

Mani M, Pillai R. 2010. Impact of dust on solar photovoltaic (PV) performance: Research status, challenges and recommendations. Renewable and Sustainable Energy Reviews, 14(9): 3124–3131.

Mertia R S, Santra P, Kandpal B K, et al. 2010. Mass–height profile and total mass transport of wind eroded aeolian sediments from rangelands of the Indian Thar Desert. Aeolian Research, 2(2–3): 135–142.

Nahar N M, Gupta J P. 1990. Effect of dust on transmittance of glazing materials for solar collectors under arid zone conditions of India. Solar & Wind Technology, 7(2–3): 237–243.

Namikas S L. 2003. Field measurement and numerical modelling of aeolian mass flux distributions on a sandy beach. Sedimentology, 50(2): 303–326.

Ni J R, Li Z S, Mendoza C. 2002. Vertical profiles of aeolian sand mass flux. Geomorphology, 49(3–4): 205–218.

Said S A M. 1990. Effects of dust accumulation on performances of thermal and photovoltaic flat-plate collectors. Applied Energy, 37(1): 73–84.

Schellenberg A, Maffei J, Telleen K, et al. 2013. Structural analysis and application of wind loads to solar arrays. Journal of Wind Engineering and Industrial Aerodynamics, 123: 261–272.

Shademan M, Barron R M, Balachandar R, et al. 2014. Numerical simulation of wind loading on ground-mounted solar panels at different flow configurations. Canadian Journal of Civil Engineering, 41(8): 728–738.

Shen Y, Wang X, Cong R, et al. 2013. Eco-geographical zoning of deserts and gobi in China. Journal of Arid Land Resources and Environment, 27(1): 1–13.

Warsido W P, Bitsuamlak G T, Barata J, et al. 2014. Influence of spacing parameters on the wind loading of solar array. Journal of Fluids and Structures, 48: 295–315.

Zhang C, Li Q, Zhou N, et al. 2016. Field observations of wind profiles and sand fluxes above the windward slope of a sand dune

before and after the establishment of semi-buried straw checkerboard barriers. Aeolian Research, 20: 59–70.

Zhang Z, Dong Z. 2013. Field Observation of Aeolian Sediment Flux in the Southeast Tengger Desert. Journal of Desert Rresearch, 23(4): 973–980.

Zhang Z, Dong Z. 2014. Characteristics of aeolian sediment transport over different land surfaces in northern China. Soil and Tillage Research, 143: 106–115.

Zhang Z, Dong Z, Li C. 2015. Wind regime and sand transport in China's Badain Jaran Desert. Aeolian Research, 17: 1–13.

Zhang Z, Dong Z, Wu G. 2017. Field observations of sand transport over the crest of a transverse dune in northwestern China Tengger Desert. Soil and Tillage Research, 166: 67–75.

Zingg A W. 1953. Some characteristics of aeolian sand movement by saltation process. Edition du Centre National de la Recherche Scientifique, 7: 197–208.

Zorrilla-Casanova J, Piliougine M, Carretero J, et al. 2013. Losses produced by soiling in the incoming radiation to photovoltaic modules. Progress in Photovoltaics, 21(4): 790–796.